



A Benchmark Study for Phase Transformation of Shape Memory Alloy Based Split Ring Resonator Structure Under a Heating and Cooling Thermal Cycle

Mehmet Mete OZTURK*

Eskişehir Technical University, Transportation Vocational School, Eskişehir
ozturkmmete@gmail.com ORCID: 0000-0003-4743-5549, Tel: (222) 335 05 80 (5140)

Bahadır DOĞAN

Eskişehir Osmangazi University, Mechanical Engineering Department, Eskişehir
bdogan@ogu.edu.tr ORCID: 0000-0003-4648-1375

Geliş: 09.05.2019, Revizyon: 02.07.2019, Kabul Tarihi: 05.09.2019

Abstract

In this benchmark study, the integration of shape memory alloy thin film on to a split ring resonator is investigated. Split ring resonators are artificially produced structures which are used to generate magnetic response. One of the applications that can be met in the literature is the solar panel ones where they are benefitted for the electric generation from the resonance of it. Unfortunately, this application is very sensitive to the shape, geometry and dimensions which can be affected from ambient conditions easily. At this particular stage, to compensate the dimensional inconsistencies by shape memory alloy thin film is chosen in an ongoing project. Due to the nature of the shape memory alloy, not only the material properties but also the geometry of the structure can also change. By taking the advantage of this unique feature, the applicability of coupling shape memory alloy thin film by split ring resonator is investigated. And as an initial step of this research, the phase transformation of shape memory alloy thin film is investigated with regard to varying ambient conditions which are simulated by the change of convection conditions and exposure time. The temperature evolution of two significant point is tracked under these conditions and furthermore the change of martensite volume fraction is examined which will enlighten the path for the further steps on this investigation.

Keywords: Shape memory alloy, split ring resonator, phase transformation, volume fraction

* Yazışmaların yapılacağı yazar

Introduction

A split-ring resonator (SRR) is an artificially produced structure which is commonly used to produce the desired magnetic response that can reach up to 200 terahertz with varying metamaterial types. This artificial structure is widely preferred when it is not possible to provide with conventional materials. There are different resonators such as split ring resonator (SRR), spiral resonator (SR), omega and fractal resonator which exhibit metamaterial characteristics (Karthikeyan and Arulvani (2010); Cetin et al. (2012)). These are widely used in different microwave applications because of their sub wavelength metallo-dielectric property that have strong resonance behavior. A cell of SRR has a pair of enclosed loops which can have different shapes such as rectangles or circles, with openings in them at opposite ends (Fig. 1) where the loops are made of nonmagnetic metal with a space between them. The shape, size and spacing of the loop vary depending on the requirement.

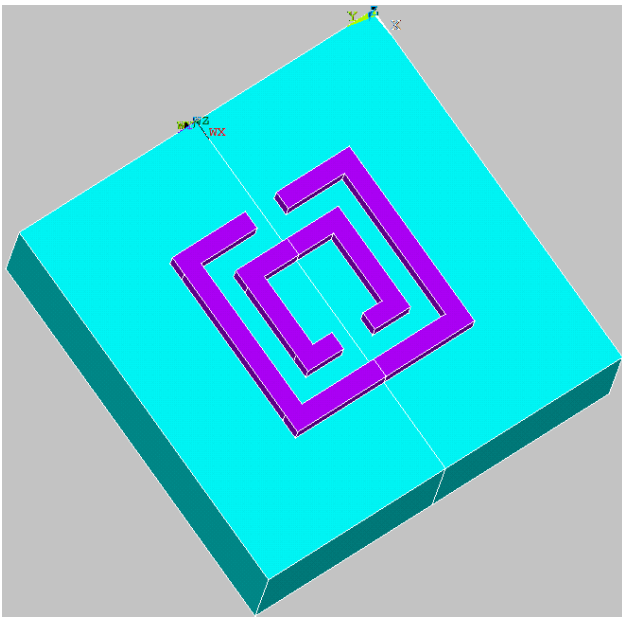


Figure 1. Split Ring Resonator geometry

In literature, researchers have investigated SRR models with different geometries and sizes. Karthikeyan and Arulvani (2010) presented open split ring resonator (OSRR) which is a modified geometry of a split ring resonator that

has negative permeability. They reported that by this structure, same frequency could be provided by a smaller resonator instead of the conventional ones.

An interdigitated split-ring resonator (ISRR) is the negative indexed resonator over in a narrow range frequency. Sohn et al. (2011) demonstrated the applicability of linear frequency response for their proposed a geometry for small planar resonators at low range of frequency. An experimental study is reported by Varadan and Ji (2010) to observe the shift in resonance frequency by a gradually increasing environmental temperature. They noted the downward shift of the resonance frequency with increasing temperatures. Cheng et al. (2010) designed, simulated and tested a tunable SRR based antenna that accomplishes better tunability and reduce the size more than conventional ones.

One other resonator application bases on metallic nanostructures gets attention in last years. Cetin et al. (2012) presented a plasmonic multiband metamaterial by using UT shaped nanoparticles. Hosseini and Massoud (2007) presented a rectangular metal-insulator-metal based on nanoscale plasmonic resonator which is designed in rectangular shape and within the spectral range of 270 nm. Okamoto et al. (2013) investigated the effect of the space between the two plasmonic racetracks of the resonator on the quality factor. On the other side, the shape memory alloys (SMA's) are the metal alloys which can return to their original shape by an external stimulus such as thermal or magnetic field applied on it and widely used for the fabrication of micro-actuators and micro-sensors. This unique feature is bases on the shape memory effect which is a solid-solid phase transformation takes place between a high temperature phase of austenite and a low temperature phase of martensite. The phase transformation usually accompanied by a temperature dependent change in material properties such as the thermal conductivity, electrical resistivity and heat capacity (Amalraj et al. (2000)). Although a wide range of materials with different maximum recoverable strains and thermomechanical properties are available, the

commercially available NiTi alloy is very popular due to its large range of recoverable deformations and its relative ease of processing. In literature it has been used for several applications including, micro-pumps, micro-grippers, micro-valves etc. (Makino et al. (2001); Kohl et al. (2000); Lee et al. (1996); Reynaerts et al. (1997); Wang et al. (2002)). Kohl et al. (2000) reported a micro-valve with 100 μm thick membrane which is made of Ti-Ni-Pd to activate the micro device. Another micro-pump was developed by Makino et al. (2001) and was composed of 6 μm thick SMA thin film deposited on a Si wafer and trained for a flat shape. Another study on valveless micro-pumps is the one designed by Lee et al. (39) and processed by deep reactive ion etching (DRIE) in silicon. Reynaerts et al. (1997) designed a drug delivery system using micro-valve made from SMA to reduce the injection of the patients with 5 μl dose control. In another work, Wang et al. (2002) reported micro-tweezers that uses the residual stress in TiNi film. Kaya (2017) investigated the effects of cooling rate after an aging process on the shape memory behavior and mechanical properties of Ti-54at.%Ni alloys. Ege et al. (2016) analyzed the displacement, velocity, time, force physical effects of SMA springs under different operating conditions.

The SRR's electromagnetic response is depended on, not only the electrical properties of the thin film but also its geometrical dimensions. Any change in the electrical properties and/or geometrical dimensions will impact the electromagnetic response. Any minor change on the dimension of the SRR will have a big impact on the performance of the resonators. So the ambient that the SRR's used in, is very critical for the sake of the performance of the system. If the SRR's are exposed to the direct sunlight such as in solar panel applications, it is open to the temperature fluctuations during the day which inclines to performance variation as a result of this dimensional change. At this stage, taking the advantage of the shape memory alloy's temperature dependent phase transformation is suggested by the researchers which can be used as absorbent of the negative impacts of the

temperature change on the SRR's caused by the sunlight during the operation of the devices.

As mentioned earlier, the basic feature of the SMA's is the temperature based transformation of the alloys which is accompanied by a change in the dimensions of the thin film as well. Thus the use of an SMA thin film which can accompany to SRR as a base layer can lead to a tunable resonator. Due to strong thermomechanical coupling in the phase transformation of these materials, knowledge of thermal field is necessary. In this particular study, the thermal behavior of SMA thin film in SRR geometry is studied under convection boundary condition as the simulation of the ambient condition in the course of a heating and cooling cycle during the exposure time. The ultimate purpose is to provide some preliminary outcomes in order to observe the phase transformation by revealing impact on it in this benchmark investigation.

Boundary value problem for SMA based SRR model

The Dimensional Problem of the SMA based SRR

The SRR structure simulated in this particular work bases on the geometry of the one cell of the SRR which is developed by Varadan and Ji (2010) which could be seen in Fig. 2. In order to simplify the calculation, the half of the developed geometry is considered and modeled (Fig. 2). The dimensions of the SRR model are taken as $v = 17\mu\text{m}$, $s=0.3\text{ mm}$, $w=0.25\text{ mm}$ and $l = 2.62\text{ mm}$ as regard to the real dimensions of the designed resonator. The theory of the model begins with the energy conservation of it, which is given below,

$$\vec{\nabla}(k(\xi)\vec{\nabla}T) + \rho(\xi)J^2 = C_v(\xi)\frac{\partial T}{\partial t} - Hp(\xi)\frac{\partial T}{\partial t} \quad (1)$$

where $\vec{\nabla}$ is the del operator, $k(\xi)$ is the thermal conductivity, $\rho(\xi)$ is the electrical resistivity and $C_v(\xi)$ is the heat capacity of the SMA thin film which are all temperature dependent. The

parameter on the right, $H_p(\xi)$, is the latent heat which is depended on the temperature evolution, besides ‘ H ’ is the net latent heat per unit volume.

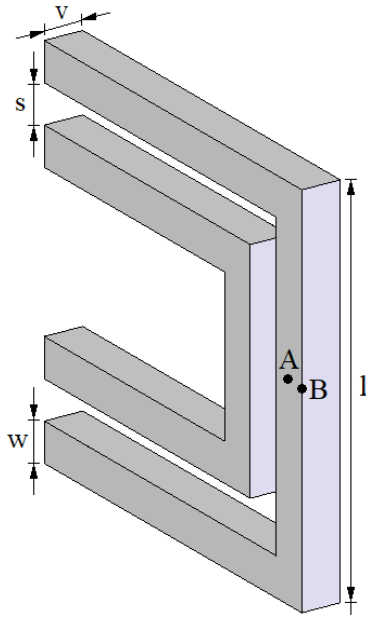


Figure 2. The schematic of the SMA based SRR model used in the study developed by considering the symmetric feature of the structure.

The material parameters for the SMA thin film which can be written with regard to phase transformation,

$$\begin{aligned}
 k(\xi) &= k_{Aus} + \xi(k_{Mar} - k_{Aus}), \\
 \rho(\xi) &= \rho_{Aus} + \xi(\rho_{Mar} - \rho_{Aus}), \\
 C_v(\xi) &= C_{v,Aus} + \xi(C_{v,Mar} - C_{v,Aus}), \\
 p(\xi) &= \frac{\partial \xi}{\partial T}
 \end{aligned}
 \tag{2}$$

where the phases austenite and martensite are shown by the subscripts ‘ Aus ’ and ‘ Mar ’, respectively. The symbol, ξ , which appears in the Eq. 1 and Eq. 2 refers to the martensite volume fraction which ranges between zero and one. When martensite volume fraction equals to 1 it corresponds to the phase where it is completely martensite and the exact opposite is true when it is equals to 0. The evolution of the volume fraction can be defined by a simple sigmoidal function which is given below,

$$\begin{aligned}
 \xi(T) &= 1 - \frac{1}{1 + e^{-[T - (A_s + A_f)]/2]/T_0}} \\
 \xi < 0, \quad A_s \leq T \leq A_f \\
 \xi(T) &= 1 - \frac{1}{1 + e^{-[T - (M_s + M_f)]/2]/T_0}} \\
 \xi > 0, \quad M_s \leq T \leq M_f
 \end{aligned}
 \tag{3}$$

where A_s , A_f , M_s and M_f are the temperatures which refers to austenite start, austenite finish, martensite start and martensite finish respectively, and ξ indicates the evolution of the martensite volume fraction with respect to time. Eq. 2 can be rewritten by considering Eq. 3 as in the following,

$$p(T) = -\xi(1 - \xi)
 \tag{4}$$

The surface of the NiTi SMA based SRR is exposed to a convective boundary condition which is defined below

$$-k \nabla T \cdot \hat{n} = h(T - T_0)
 \tag{5}$$

where ‘ h ’ is the convection coefficient and T_0 is the ambient temperature. At $\bar{z} = 0$ (the bottom surface of the SMA based SRR model), there is an adiabatic condition

$$\vec{q} \cdot \hat{n} = 0
 \tag{6}$$

The Non-Dimensional Problem of the SMA based SRR

In order to simplify the problem during the calculations and have a better perspective at the end of the runs by providing more generalized outcomes, the governing equations and the boundary conditions are rewritten in non-dimensional form as in the following. It is worth to note that, the non-dimensional quantities are indicated with an overbar. The non-dimensional temperature field and non-dimensional length dimensions associated with the SRR model are given below,

$$\bar{T} = \frac{T - T_0}{T_0}, \quad \bar{v} = 1, \quad \bar{s} = \frac{s}{v}$$

$$\bar{w} = \frac{w}{v} \quad , \quad \bar{l} = \frac{l}{v} \quad (7)$$

where length dimensions are non-dimensionalized with respect to the thickness, v . The governing equation is nondimensionalized as in the following,

$$\vec{\nabla}(\bar{k}(\xi)\vec{\nabla}\bar{T}) + \bar{\rho}(\xi)\bar{J}^2 = \bar{C}_v(\xi)\frac{\partial\bar{T}}{\partial\bar{t}} - \bar{H}\bar{p}(\xi)\frac{\partial\bar{T}}{\partial\bar{t}} \quad (8)$$

The material properties of the martensitic form of the NiTi SMA is benefited during non-dimensionalization, the obtained parameters are given below,

$$\begin{aligned} \bar{t} &= \frac{k_{Mar}}{L_{max}^2 C_{v,M}} t \quad , \quad \bar{J}^2 = \frac{\rho_{Mar} L_{max}^2}{T_0 k_{Mar}} J^2 \\ \bar{H} &= \frac{1}{C_{v,Mar} T_0} H \quad , \quad \bar{h} = \frac{L_{max}}{k_{Mar}} h \end{aligned} \quad (9)$$

In the same manner, the non-dimensional parameters are defined below

$$\begin{aligned} \bar{k}(\xi) &= \frac{k_{Aus} + \xi(k_{Mar} - k_{Aus})}{k_{Mar}} \\ \bar{\rho}(\xi) &= \frac{\rho_{Aus} + \xi(\rho_{Mar} - \rho_{Aus})}{\rho_{Mar}} \\ \bar{C}_v(\xi) &= \frac{C_{v,Aus} + \xi(C_{v,Mar} - C_{v,Aus})}{C_{v,Mar}} \\ \bar{p}(\xi) &= p(T)T_0 \end{aligned} \quad (10)$$

The equations regarding the volume fraction (Eq. 3-6) can be rewritten by considering the non-dimensional parameters as in the following,

$$\begin{aligned} \xi(\bar{T}) &= 1 - \frac{1}{1 + e^{-[\bar{T} - (\bar{A}_s + \bar{A}_f)/2]}} \\ \xi < 0 \quad , \quad \bar{A}_s \leq \bar{T} \leq \bar{A}_f \\ \xi(\bar{T}) &= 1 - \frac{1}{1 + e^{-[\bar{T} - (\bar{M}_s + \bar{M}_f)/2]}} \\ \xi > 0 \quad , \quad \bar{M}_s \leq \bar{T} \leq \bar{M}_f \end{aligned}$$

$$\begin{aligned} (-\bar{k}\vec{\nabla}\bar{T}) \cdot \hat{n} &= \bar{h}\bar{T} \\ \vec{q} \cdot \hat{n} &= 0 \quad or \quad \bar{T} = 0 \end{aligned} \quad (11)$$

Material properties and non-dimensional parameters used in the study

In ideal cases, it would be the best to use the accurate material properties of the austenite and martensite of thin film investigated in the study. But it is very challenging to identify these properties for thin films and unfortunately, an accurate determination for all the necessary features such as – mechanical and electrical - is not available, for this particular work. So the findings from the communication of Amalraj et al. (2000), which is about the material properties of shape Memory Alloy, are benefited during the calculations. In the mentioned work, the material properties are reported for NiTi wires for austenite and martensite individually such as;

- Thermal conductivity: $k_{Aus} = 28 \text{ W/(mK)}$,
 $k_{Mar} = 14 \text{ W/(mK)}$
- Electrical resistivity: $\rho_{Aus} = 8.371 \times 10^{-4} \Omega \cdot \text{mm}^{-1}$,
 $\rho_{Mar} = 9.603 \times 10^{-4} \Omega \cdot \text{mm}^{-1}$
- Heat capacity: $C_{v,Aus} = 5.92 \times 10^6 \text{ J/(Km}^3)$,
 $C_{v,Mar} = 4.50 \times 10^6 \text{ J/(Km}^3)$

In the same study martensite start and finish temperatures, austenite start and finish temperatures are reported as $M_s=333 \text{ K}$, $M_f=323 \text{ K}$, $A_s=345 \text{ K}$ and $A_f=355 \text{ K}$, respectively which are listed in Table 1.

The ambient temperature is assumed as $T_o=293 \text{ K}$. The dimensional convection coefficient used in the study is $2 \times 10^7 \text{ W/m}^2$ due to the nature of the small surface area investigated in the work. The non-dimensional form of this coefficient is obtained as 2.42 with regard to the normalization path described in previous section.

Table 1. Phase transformation temperatures

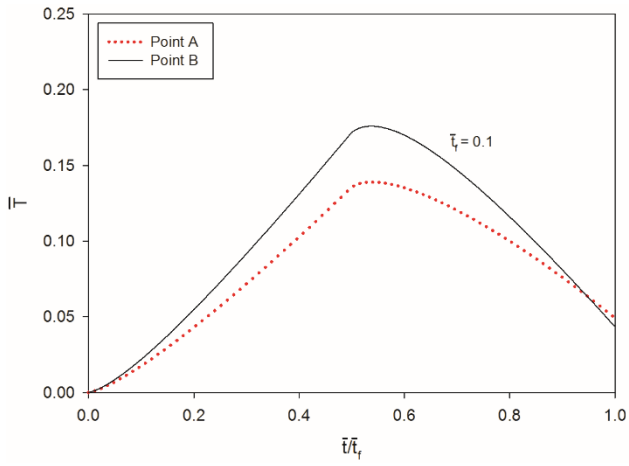
Phase Transformation	Temperature (K)
M_s	333
M_f	323
A_s	345
A_f	355

Results and Discussion

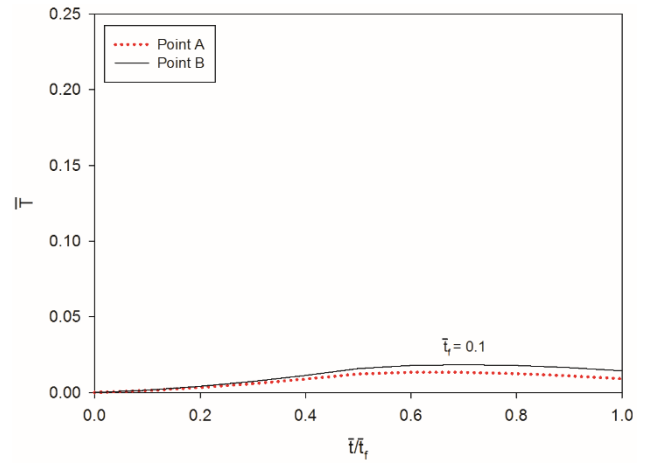
The results are generated by finite element software ABAQUS with the implementation of a subroutine UMATHT in order to control the change in material properties due to temperature variation during analysis. The material properties used in the analysis are explained in the previous section. The dimensions and material properties used during the calculations are explained in detail in section 2. In this particular work, the evolution of the SMA based SRR structure's phase transformation is examined under convection boundary condition as the basic simulation approach of the heating of the SRR structure by sun. Since the ultimate goal is to provide preliminary information for an ongoing project about where and how the SMA based SRR structure transforms under determined ambient conditions, two heat transfer coefficients ($h=2.42$ and 0.242) and three different exposure times ($\bar{t}_f=0.1, 10$ and 100) are considered. Under the given conditions, transformation response of the SMA based SRR structure is observed whether the structure transforms uniformly under poor weather conditions. The SMA based SRR is exposed to convection which would act like the heat source and heat sink of the model during the exposure time as the representative of the ambient conditions in real applications. Different convection conditions are studied, to see the impact of it on the thermal response and phase transition of SMA based SRR where the non-dimensional temperature is kept as 0.21 which marginally above the austenite finish temperature of the shape memory alloy. The temperature evolution for $\bar{h}=2.42$ is presented in Fig. 3a-3c for three different exposure times where the half of the considered period pertains to heating while the remaining half pertains to cooling. The temperature evolution is presented for two different points, Point A and Point B, which are chosen to present the evolution on the highest temperature region (edge of the structure) and lowest temperature region (mid part of the surface). Since the exposure times are different in each case, temperature evolution is given for normalized times scaled with respect to total

exposure time, \bar{t}_f , which has been taken as $0.1, 10$ and 100 respectively.

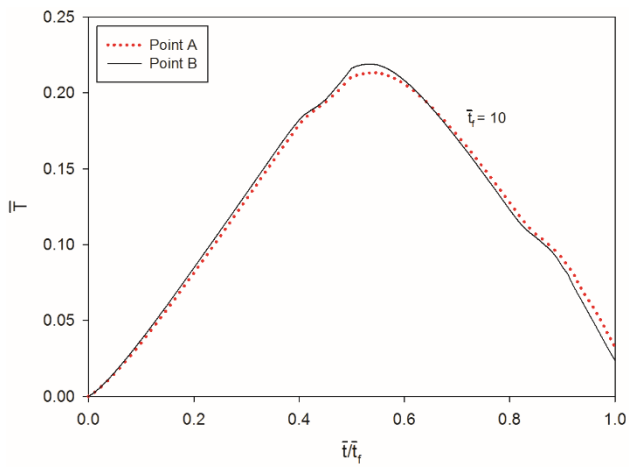
As it is seen from the figures, for the shorter period of time (Fig. 3a) even though the temperatures at the points weren't able to attain to reach the transformation temperature, the temperatures for either point rises by regarding the increment on the boundary condition, in addition the difference between the point A & B tells the entire structure's temperature couldn't be uniform in such that short application times. As the exposure time increases (Fig. 3b) the SRR model achieves to reach to transformation temperatures and along with the longer period the uniformity of the temperature distribution gets better and during the longest exposure time a linear smooth evolution is observed and it can be noted that, the temperature distribution occurs uniformly since the difference between the two points is marginal. The temperature evolution for $\bar{h}=0.242857$ –an order magnitude lower- is presented in Fig. 4a-4c for three different exposure times as well, where the half of the duration pertains to heating and the other half pertain to cooling once again. The temperature evolution is presented as a comparison between the point A and point B. Temperature evolution is given for normalized time scaled with respect to final time of each case which are $0.1, 10$ and 100 respectively. As it is demonstrated in Fig. 4a, at $\bar{t}_f=0.1$, the maximum attained temperature is far below the transformation range which shows for this poor convection conditions, given time is not enough to develop a transformation. In Fig.4b the convection time is $\bar{t}_f = 10$ and even though temperature could achieve to reach the transformation start temperature, it couldn't attain to finish temperature. Besides the temperature difference at two points presents the non-uniformity of the temperature distribution. Finally temperature evolution for the convection time $\bar{t}_f = 100$ at points A & B is presented in Fig. 4c, where the temperatures were able to reach to transformation range with a marginal difference from each. From this point It can be noted that the transformation of the entire model has a relatively uniform temperature distribution.



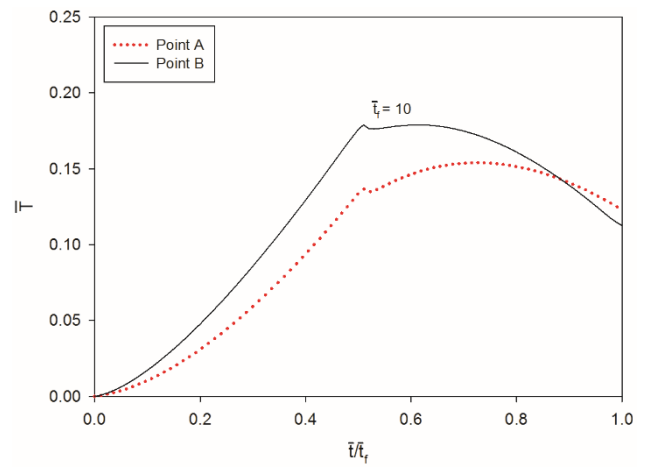
(a)



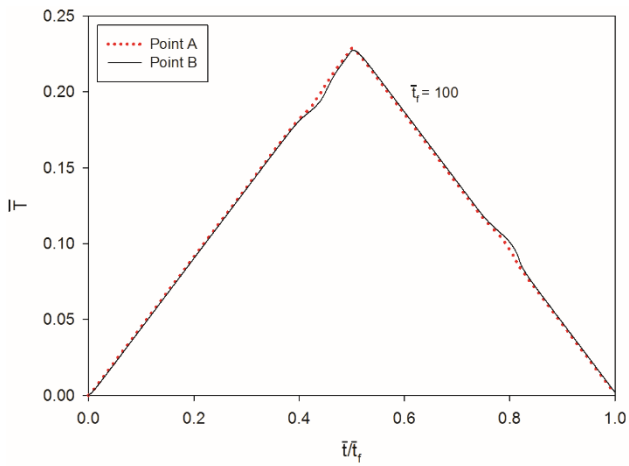
(a)



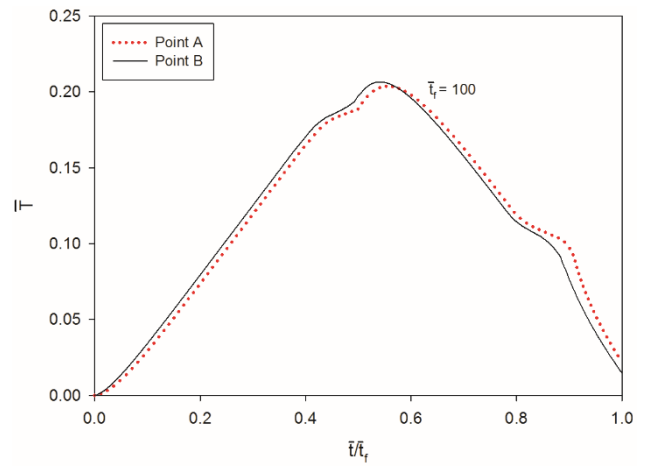
(b)



(b)



(c)



(c)

Figure 3. Non dimensional temperature evolutions with respect to normalized time scaled with respect to exposure time with $h=2.42$ (a) $\bar{\tau}_f=0.1$, (b) $\bar{\tau}_f=10$ and (c) $\bar{\tau}_f=100$.

Figure 4. Non dimensional temperature evolutions with respect to normalized time scaled with respect to exposure time with $h=0.242$ (a) $\bar{\tau}_f=0.1$, (b) $\bar{\tau}_f=10$ and (c) $\bar{\tau}_f=100$.

In Fig. 5 and 6, the temperature contour plot of two sets of simulations are demonstrated. The first one pertains to simulation with $\bar{h}=2.42$ during $\bar{t}=100$ and the latter belongs to the simulation with $\bar{h}=0.242$ during $\bar{t}=0.1$. As given on the graphs, the highest temperatures are observed for the higher convection value which occurs in longer period along the same path given

in Fig. 3. Even though the contour plots for the second figure are looking almost identical, it should be noted that same plot range is used with the first graph which leads to such that visual resemblance between the contours of different time frames which presented in Fig. 3 as well, where the temperature values are very small with regard to longer exposure times in Fig. 4c.

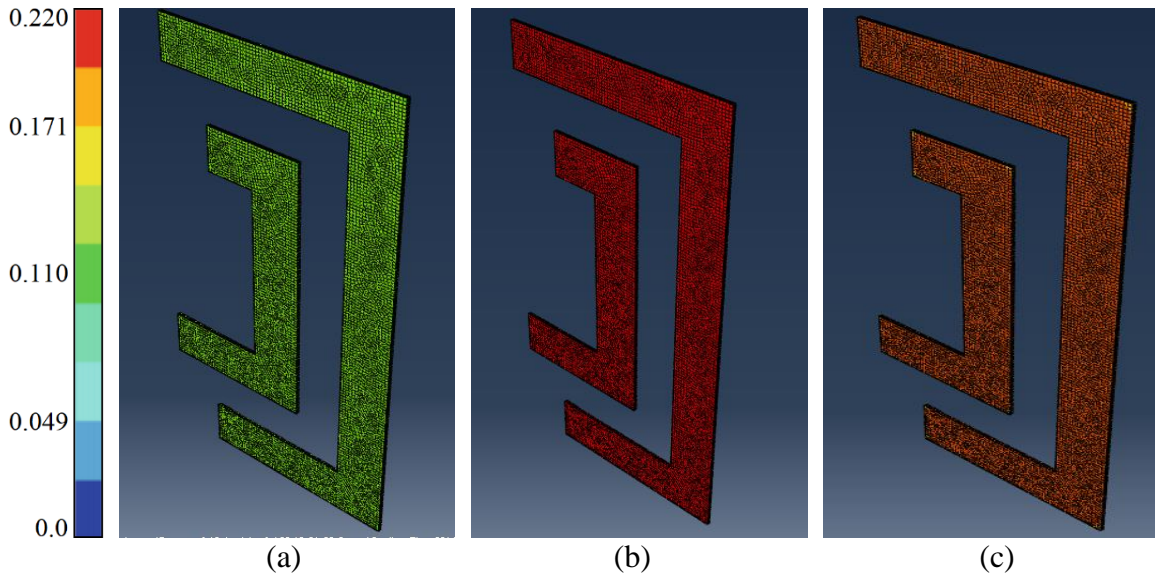


Figure 5. Contour plot of non-dimensional temperature for $\bar{h}=2.42$ with a convection time $\bar{t}_f=100$ at normalized times (a) $\bar{t}/\bar{t}_f=0.25$, (b) $\bar{t}/\bar{t}_f=0.5$ and (c) $\bar{t}/\bar{t}_f=0.75$.

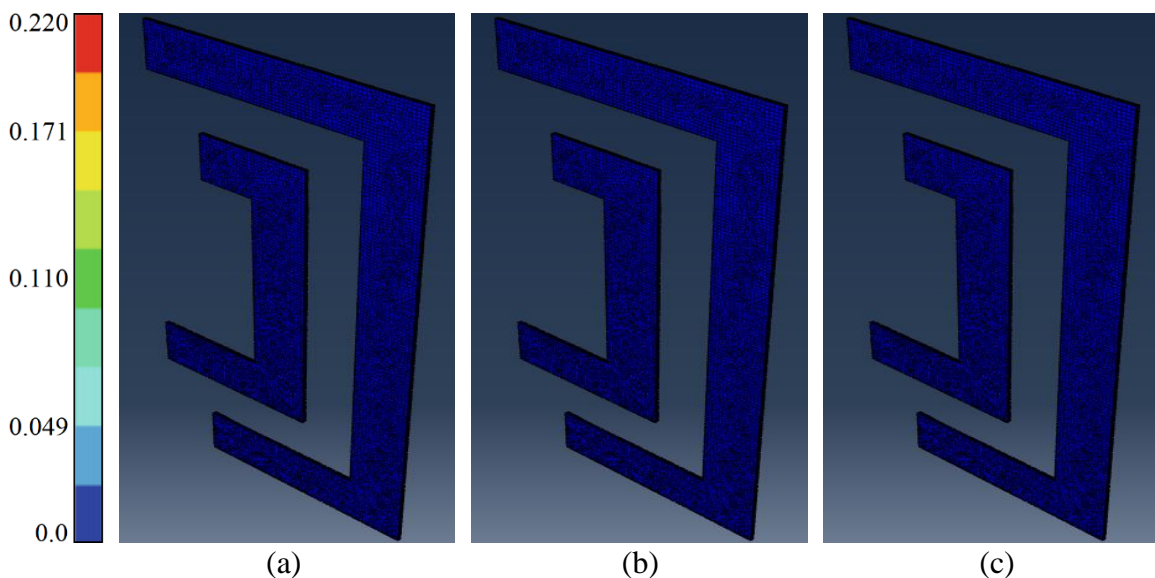


Figure 6. Contour plot of non-dimensional temperature for $\bar{h}=0.242$ with a convection time $\bar{t}_f=0.1$ at normalized times (a) $\bar{t}/\bar{t}_f=0.25$, (b) $\bar{t}/\bar{t}_f=0.5$ and (c) $\bar{t}/\bar{t}_f=0.75$.

From the figures, it is obvious that, when the heat transfer ambient becomes worsen at very low exposure times, the conditions are not sufficient to transform the entire structure as in the better conditions ($\bar{h}=2.42$ during $\bar{t}=100$). Since the simulations are carried out for different convection times in order to provide a comparison between the transformation responses of the simulations, normalized time is used in the same manner given earlier.

The martensite volume fraction evolution for varying exposure times with respect to normalized non dimensional time is presented in Fig. 7. The volume fraction is given as the average martensite ratio of the entire SRR structure. Since the SMA based SRR model calculations for $\bar{h}=2.42$ with $\bar{t}=0.1$ and for $\bar{h}=0.242$ with $\bar{t}=0.1$ & $\bar{t}=10$ couldn't achieve to

complete the transformation, they are not included to the figure.

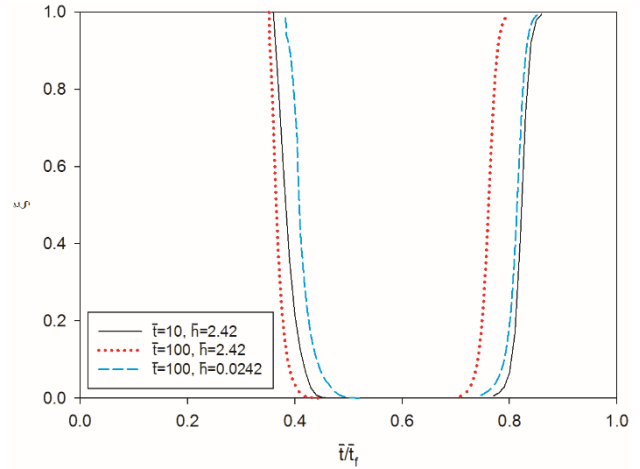


Figure 7. Evolution of martensite volume fraction scaled with different exposure times.

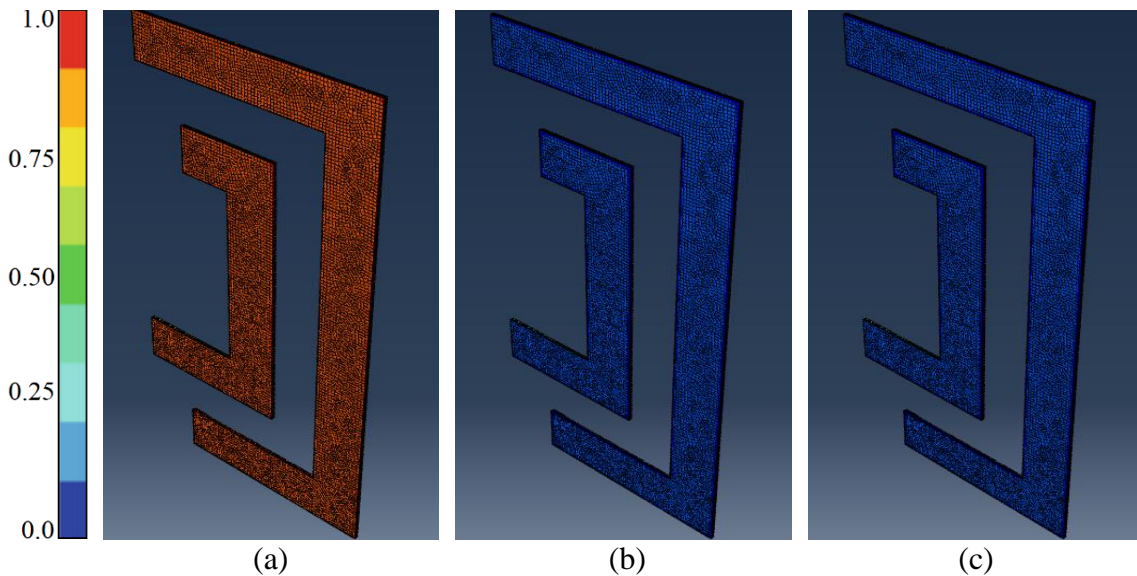


Figure 8. Contour plot of martensitic volume fraction for $\bar{h}=2.42$ with an exposure time $\bar{t}_f=100$ at (a) $\bar{t}/\bar{t}_f=0.25$, (b) $\bar{t}/\bar{t}_f=0.5$ and (c) $\bar{t}/\bar{t}_f=0.75$.

In the figure, martensite volume fraction evolves between 1 and 0 where they are corresponding to fully martensite and fully austenite phases respectively. Martensite volume fraction is the measure, which shows the part of the geometry that accomplishes to transform from austenite to martensite. As it is seen the SRR model with longer exposure time completes the transformation either from martensite to austenite or austenite to martensite quicker than the other conditions according to the normalized

non dimensional time. To complete the transformation from martensite to austenite the convection with lower coefficient requires more time then the simulations with higher coefficients as expected but according to the normalized time it can complete the transformation from austenite to martensite about the same time range with the case $\bar{h}=2.42$ with $\bar{t}=10$. The change of martensitic volume fraction over the normalized time is given by contour plots for the simulation with $\bar{h}=2.42$ during $\bar{t}=100$ in Fig. 8. The SRR

hasn't started to turn its phase and still in martensite at $\bar{t}=0.25$ which is represented by red color, in the next frame which shows the volume fraction at $\bar{t}=0.5$, it is seen that entire SRR completes its transformation and color turns to blue. In final frame which pertains to volume fraction at $\bar{t}=0.75$, the color of the SRR model remains blue since the transformation starts just beyond this limit and at the given time the phase of the structure is still austenite. This evolution can be followed from the Fig. 7 where the average volume fraction change is summarized.

Conclusion

This study is a benchmark investigation as a part of an ongoing project, in which the shape memory alloy thin films are planned to be coupled with split ring resonators in order to improve the performance of them. One of the early steps of this investigation is to identify thermal response of the SMA based SRR structure under varying ambient conditions and try to provide preliminary information about the behavior under several conditions.

In this particular work, the SMA based geometry's response is examined under different convection boundary condition for several exposure times as the correspondent of the varying ambient conditions. As regard to the outcomes, when the heat transfer coefficient which represents a better ambient condition, has higher values, the transformation of the geometry becomes easier and uniformly. Besides when the exposure time gets longer, geometry finds enough time to transform uniformly instead of partial transformation which can happen in shorter periods of time. It is obvious from the findings that; the exposure time should be extended to provide the full transformation in worse weather conditions.

Acknowledgement

We are grateful to Dr. A. Bhattacharyya (University of Arkansas at Little Rock) for his contribution by supervising the research.

Nomenclature

A_f	austenite finish temperature, K
A_s	austenite start temperature, K
C_v	heat capacity, $\text{JK}^{-1}\text{m}^{-3}$
\bar{C}_v	dimensionless heat capacity
h	heat transfer coefficient, $\text{Wm}^{-2}\text{K}^{-1}$
\bar{h}	dimensionless form of h
H	net latent heat per unit volume, kJ/m^3
\bar{H}	dimensionless form of H
J	current density
\bar{J}	non-dimensional current density
k	thermal conductivity, $\text{Wm}^{-1}\text{K}^{-1}$
\bar{k}	dimensionless form of k , $\text{Wm}^{-1}\text{K}^{-1}$
L_{max}	film thickness, μm
l	dimension of the SRR, mm
\bar{l}	dimensionless form of l
M_f	martensite finish temperature, K
M_s	martensite start temperature, K
\hat{n}	unit vector
\vec{q}	heat flux, W/m^2
s	dimension of the SRR, mm
\bar{s}	dimensionless form of s
T	temperature, K
\bar{T}	dimensionless temperature
T_0	ambient temperature, K
t	time, s
\bar{t}	dimensionless time
v	dimension of the SRR, mm
\bar{v}	dimensionless form of v
w	dimension of the SRR, mm
\bar{w}	dimensionless form of w

Greek letters

ξ	martensite volume fraction
ρ	electrical resistivity, $\Omega.\text{mm}^{-1}$
$\bar{\rho}$	dimensionless electrical resistivity

Appendix A: User Defined Subroutine for Abaqus (UMATHT)

The challenging point about the calculations is, using the right material properties at a given point and time for phase transformation's evolution during heating cooling thermal cycle. At any particular location, the material properties rely on the present phase of the location, or in

another word, depends on the volume fraction of phase which is connected to the local temperature of the structure. So it is very important to implement the volume fraction dependent material properties to the calculations.

In ABAQUS, UMATHT subroutine allows to do such calculations. Thus, the rate of change of internal energy is written as

$$\rho \frac{du}{dt} = \rho C_v(\xi) \frac{\partial T}{\partial t} - Hp(\xi) \frac{\partial T}{\partial t} - \rho(\xi) J^2 \quad \text{A.1}$$

where “ u ” is the internal energy per unit mass. Time discretization represented by $du / dt \sim \Delta u / \Delta t$, we have

$$\Delta u = \left(\rho C_v(\xi) - H \frac{\partial \xi}{\partial T} \right) \Delta T - \rho(\xi) J^2 \Delta t \quad \text{A.2}$$

Given equations and more are used in the subroutine, UMATHT. For details of the implementation, the reader is referred to Ozturk (2015)

References

- Amalraj, J.J., Bhattacharyya, A., Amalraj, J.J., Faulkner, M.G., 2000. Finite-element modeling of phase transformation in shape memory alloy wires with variable material properties. *Smart Materials and Structures* 9(5), 622-631.
- Cetin, A.E., Turkmen, M., Aksu, S., Altug, H., 2012. Nanoparticle-Based Metamaterials as Multiband Plasmonic Resonator Antennas, *Proceedings, IEEE Transactions on Nanotechnology*, 208-212,
- Cheng, X., E., S.D., Whalen, J.J., Yoon, Y.-K., 2010. Electrically small tunable split ring resonator antenna, *Proceedings, 2010 IEEE Antennas and Propagation Society International Symposium*, Toronto, ON, Canada.
- Ege, G.K., Akkus, N., Ege, M., 2016. Analysis of Mechanical Properties of Shape Memory Alloy. *International Journal of Applied Mathematics, Electronics and Computers*, 240-240.
- Hosseini, A., Massoud, Y., 2007. A rectangular metal-insulator-metal based nanoscale plasmonic resonator, *Proceedings, 2007 7th IEEE Conference on Nanotechnology (IEEE NANO)*, 81-84, Hong Kong, Hong Kong.
- Karthikeyan, S.S., Arulvani, M., 2010. Double negative metamaterial design using open split ring resonator, *Proceedings, 2010 IEEE Students Technology Symposium (TechSym)*, Kharagpur, India.
- Kaya, I., 2017. Effect of cooling rate on the shape memory behaviour of Ti-54at.%Ni alloys. *Anadolu Universtiy Journal of Science and Technology A - Applied Sciences and Engineering*.
- Kohl, M., Dittmann, D., Quandt, E., Winzek, B., 2000. Thin film shape memory microvalves with adjustable operation temperature. *Sensors and Actuators A: Physical* 83(1-3), 214-219.
- Lee, A.P., Ciarlo, D.R., Krulevitch, P.A., Lehew, S., Trevino, J., Northrup, M.A., 1996. A practical microgripper by fine alignment, eutectic bonding and SMA actuation. *Sensors and Actuators A: Physical* 54(1-3), 755-759.
- Makino, E., Mitsuya, T., Shibata, T., 2001. Fabrication of TiNi shape memory micropump. *Sensors and Actuators A: Physical* 88(3), 256-262.
- Okamoto, H., Onishi, S., Kataoka, M., Yamaguchi, K., Haraguchi, M., Okamoto, T., 2013. Characteristics of double-plasmonic-racetrack resonator to increase quality factor. *Optical Review* 20(1), 26-30.
- Ozturk, M.M., 2015. Thermal Modeling and Nano Indentation of Shape Memory Alloy Thin Films, *PhD*, University of Arkansas at Little Rock, Mississippi, USA.
- Reynaerts, D., Peirs, J., Van Brussel, H., 1997. An implantable drug-delivery system based on shape memory alloy micro-actuation. *Sensors and Actuators A: Physical* 61(1-3), 455-462.
- Sohn, S.-M., Vaughan, J.T., Gopinath, A., 2011. An interdigitated split-ring resonator for metamaterials. *Microwave and Optical Technology Letters* 53(1), 174-177.

- Varadan, V.V., Ji, L., 2010. Temperature Dependence of Resonances in Metamaterials. *IEEE Transactions on Microwave Theory and Techniques* 58(10), 2673-2681.
- Wang, R.X., Zohar, Y., Wong, M., 2002. Residual stress-loaded titanium–nickel shape-memory alloy thin-film micro-actuators. *Journal of Micromechanics and Microengineering* 12(3), 323-327.